Korean J. Chem. Eng., 40(1), 255-266 (2023)
DOI: 10.1007/s11814-022-1251-8

pISSN: 0256-1115
eISSN: 1975-7220

Modification of activated carbon from agricultural waste lotus leaf and its adsorption mechanism of beryllium

Xu Zhao[*,‡], Yucheng Su[,‡], Hongqiang Wang[**], Zhiwu Lei[**,***], Eming Hu[**], Fang Hu[**], Qingliang Wang[**,†], Lechang Xu[****,†], Shiyao Fan[**], Xinwei Liu[**], and Xuanzhang Hao[**]**

*School of Nuclear Science and Technology, University of South China, Hengyang 421001, Hunan, China
**School of Resource Environment and Safety Engineering, University of South China, Hengyang 421001, Hunan, China
***State Key Laboratory of Nuclear Resources and Environment (East China University of Technology), Nanchang, 330013, Jiangxi, China
****Beijing Research Institute of Chemical Engineering and Metallurgy, CNNC. Tongzhou District, 101149, Beijing, China
(*Received 26 April 2022 • Revised 27 July 2022 • Accepted 6 August 2022*)

Abstract−With the wide application of beryllium globally, industrial wastewater has rapidly increased. Previously, adsorption was effective in treating this issue. However, most adsorbents have a poor removal rate, primarily in the low adsorption capacity. To remove Be from industrial wastewater and overcome the disadvantages of low adsorption capacity and poor removal rate of existing adsorbents, typical agricultural waste lotus leaf was used to prepare Al-activated carbon (Al-AC) by the impregnation-calcination modification of $Al(NO_3)_3$. The theoretical maximum adsorption capacity of Al-AC was 32.86 mg/g. Langmuir, Freundlich, and Temkin models were used to thermodynamically analyze Al-AC, and adsorption thermodynamics demonstrated that the adsorption reaction of Al-AC was endothermic. Through characterization analysis, the specific surface area of the modified AC increased from 4.3573 to 155.87 m^2/g. This study provides a new approach to preparing and modifying AC and a new method for removing Be from industrial wastewater.

Keywords: Langmuir Freundlich Beryllium Activated Carbon

INTRODUCTION

Beryllium is a type of national strategic reserve resource. Because of its lightweight and high strength, Be is extensively used in nuclear weapons, nuclear reactors, inertial guidance elements, X-ray tubes, space optics, microelectronics, and other fields. Presently, China's Be external dependence is 85% [1]. With the increasingly widespread use of Be, the amount of Be mining has increased. A large amount of process wastewater, tailings' wastewater, ore washing, sedimentation wastewater, leaching water for dust removal and purification devices, floor washing in operation areas, and equipment washing wastewater are generated in the process of Be beneficiation, and wastewater from washing work clothes [2], which would pollute the surface water and groundwater resources in the surrounding environment. Be is also toxic; pure Be is not highly toxic, but some Be compounds are highly toxic and are harmful to plants and humans. It reduces plant growth by reducing seed germination [3], root length, and dry weight. Long-term human exposure to Be could cause many health problems, including granulomatous chronic Be disease, serious lung effects, and even carcinogenic risk [4]. The interaction between Be and the human immune system leads to hypersensitivity reactions with different clinical symptoms: allergic immune reaction (Be sensitization), acute Be disease (ABD), and chronic Be disease (CBD) [5].

The main treatment methods for Be are the biological, precipitation, and adsorption methods. The materials commonly used in biological methods include activated sludge [6], chlorella [7], and bacteria [8], and the results show that the removal rate exceeds 80%. However, the adsorption capacity of biosorbents is low. The precipitation method mainly adjusts the pH to 6.0-9.0 by adding an alkaline precipitation agent [9-11] to achieve the effect of Be precipitation, but the alkali precipitator pollutes water. The adsorption method mainly uses Kaolin zeolite powder [12], activated carbon (AC) [13], and sodium hydroxide modified rice husk [14] to treat Be-containing wastewater. Among them, the removal rate of Be from kaolin zeolite powder exceeds 98%. In contrast, the removal rate of AC and modified rice husk falls below 60%. Thus, the adsorption effect of AC on Be is poor. It has been reported that the removal rate of biomass-derived AC exceeds that of coal-derived AC [15]. To improve the adsorption performance of AC, many scholars have tried to modify AC. For example, the absorption of Cr by AC from date press cake [16], the adsorption of phenol by AC prepared from black wattle bark waste [17], the hydrophobicity of AC improved [18]. The cation adsorption performance of AC modified by anionic surfactants-sodium lauryl sulfate (SLS) with anionic surfactant was significantly improved [19]. Some AC is modified by loading metal cations, such as Fe [20-22], Al [23], and Cu. For example, magnetite-coated Elaeis Guineensis Jacq Shell AC (ACA-Fe_3O_4) was used to treat wastewater containing Ni^{2+} [20]. Furthermore, Al-ZnLDHS

†To whom correspondence should be addressed.
E-mail: 670566869@qq.com, xu_lechang@163.com
‡Xu Zhao and Yucheng Su contributed equally to this work.

composite AC was used to remove nitrate and phosphate [23].

Presently, most studies have shown that the adsorption effect of AC for Be is poor, and there is no report about the use of agricultural waste lotus leaves to make AC and modified as Be adsorption adsorbent. In addition, some articles [24,25] have reported that metal oxide nanoparticles can adsorb beryllium. Thus, this study uses aluminum nitrate modified lotus leaf activated carbon method to prepare adsorbent and provides a new idea for treating and disposing solid waste, which benefits environmental protection.

This study aims to explore the potential of extracting AC from lotus leaf and removing Be from aqueous solution after modification. Therefore, herein, AC was prepared under different modification conditions. The optimum AC was characterized, and its kinetics and thermodynamics were discussed.

MATERIALS AND METHODS

1. Materials

The materials include analytical pure Ethylenediamine tetraacetic acid (EDTA), pure sulfuric acid (H_2SO_4), pure hydrochloric acid (HCl), pure ammonia water ($NH_3 \cdot H_2O$), pure sodium hydroxide (NaOH), nitric acid (HNO_3), lotus leaf, and Beryllium oxide (BeO) that were purchased from Sinopharm Chemical Reagent Co., Ltd.

BeO of 0.0694 g was dissolved in 500 mL of deionized water to obtain 50-mg/L Be^{2+} standard solutions.

2. Experimental Design

In this experiment, response surface methodology (RSM) was adopted. Design-expert 13.0 software was used to Design a three-factor and three-level response surface experiment with Al^{3+} addition (X_1), adsorbent amount (X_2) and initial pH (X_3) as independent variables and the adsorption rate of Beryllium by Al-AC as response value, Y_1. The experimental coding was shown in Table 1. F-value test was used to explain the coefficients [26]. Analysis of variance (ANOVA) was used to determine the significance of each model item. The optimum conditions for Al-AC treatment of beryllium wastewater were determined by regression analysis.

3. Modified AC Preparation

Agricultural waste lotus leaves were collected as the raw material, dried, ground using a crusher, and weighed. The biomass obtained was taked 50 g and impregnated with 53 mL nitric acid solution. First, the lotus leaf powder was ground and dried at 105 °C for reserve. Afterward, 50-g dried lotus leaf powder was added to 53-mL concentrated nitric acid. Next, 50-mL water was added to the resulting mixture with stirring for 2 h, and then maceration for 15 h. The above impregnated and filtered powder was dried at 105 °C for 24 h, then placed in a tubular resistance furnace and heated up under N_2 protection of (flow rate of 100 mL/min) at a heating rate of 5 °C/min. Afterward, it underwent a constant temperature activation at 600 °C for 2 h. After the activation, N_2 was continuously passed until the furnace tube temperature was room temperature to obtain AC primary products. The products were washed using deionized water until neutrality was obtained. Additionally, the washed sample was dried at 105 °C to obtain the biochar carrier AC. The mass of AC is 15 g.

$Al(NO_3)_3$ was taked 2.25 g and dissolved in 20 mL deionized water and uniformly added to the lotus leaf biochar using the ultrasound-assisted impregnation method. After ultrasonic treatment for 120 min and drying at 105 °C for 16 h, the powder was roasted under a nitrogen atmosphere at 600 °C at a heating rate of 5 °C/min and a holding time of 2 h. The mass of $Al(NO_3)_3$ in the catalyst was 15% that of AC. The mass of Al-AC is 15.5 g, and the yield was 31%.

Table 1. Factor and level of Al-AC

Factor	Codes	Units	Level	
			Low	High
Initial pH	A (X_1)	-	1	8
Al^{3+} addition	B (X_2)	%	0	0.25
Dosage	C (X_3)	g/L	0.2	4

4. Characterization

The specific surface area was obtained by the Brunauer-Emmett-Teller (BET) (Micromertcs ASAP2460, USA) method, and pore size distribution was obtained by Barrett-Joyner-Halenda (BJH) method. The surface morphology of the AC modified from lotus leaf biomass was studied using scanning electron microscopy (SEM) (Zeiss SGMA 300, Germany). The functional group information of the AC from lotus leaf biomass was studied using Fourier transform infrared spectroscopy (FTIR, PE FTIR Frontier, USA).

RESULTS AND DISCUSSION

1. Characterization

1-1. FTIR Analysis

Surface oxygen functional groups contribute significantly to adsorption because they act as active sites to capture adsorbents [27]. Boehm provided qualitative and quantitative information on the oxygen-containing groups on the surface of carbon-based materials. This approach assumes that groups of different acids could be neutralized by bases of different strengths [28]. The adsorption capacity of Al-AC depends on the porosity and chemical reactivity of the surface functional groups. Fig. 1 shows that the hydroxyl

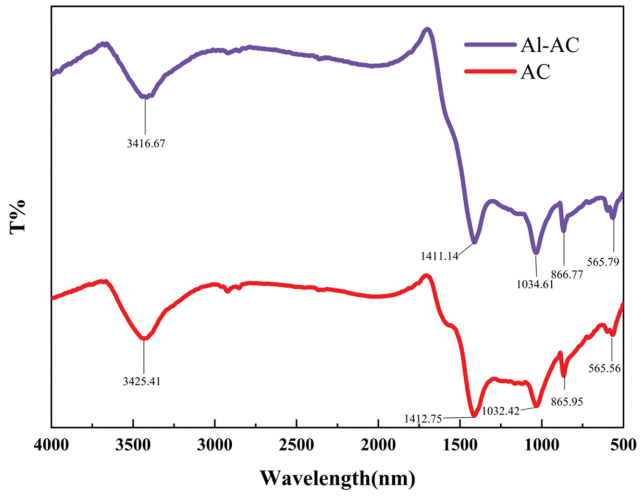

Fig. 1. FT-IR spectrum of Al-AC.

and amino groups stretch between 3,100 and 3,500 cm^{-1} [29]. The band at 1,412 cm^{-1} assigned to C-C stretching [29]. The band at 1,034 cm^{-1} (phospho-hydrogen) in the raw material spectrum is characteristic of phosphodiesterase [30]. The peak at 813 cm^{-1} indicated the presence of a C-F_2 group [31]. The FTIR spectroscopy shows that several functional groups in Al-AC could combine with heavy metal ions, especially Be^{2+}.

1-2. BET Analysis

The pore distribution curves of AC and Al-AC and the N_2 adsorption-desorption isotherms are shown in Fig. 2. The adsorption isotherms before the modification are typical of type (III), whereas the modified Al-AC is typical of type (II), which is typical of mesoporous solids [32]. In the relative pressure range of 0.8-1.0, the N_2 adsorption capacity of AC increased rapidly, indicating that no discernible monolayer was formed on the AC surface. The adsorbate-adsorbent interaction was relatively weak, and the adsorbed molecules gathered in the most favorable position on the nonporous or macroporous solid surface. Al-AC increased slowly in the relative pressure range of 0-1.0, and the unrestricted monolayer-to-multilayer adsorption indicated that the adsorption overlapped with monolayer coverage and multilayer adsorption results. Before modification, the specific surface area of AC was 4.3573 m^2/g, and the pore size was mostly medium. Also, the specific surface area of Al-AC increased to 155.87 m^2/g, the total pore volume increased to 0.061 cm^3/g, and the pore size of AC is 12.788 nm, and that of Al-AC is 3.659 nm, mainly because Al^{3+} is attached to the AC surface and pores in the soaking process, which leads to the reduction of pore size and increase of specific surface area [33]. The pore size reduction shows that the Al was successfully loaded in the AC pores, indicating that the the preparation process changed the AC surface structure to a certain extent. The specific surface area and active adsorption sites of Al-AC increase after treatment, and it has better adsorption performance [34].

1-3. XRD Analysis

The X-ray diffraction (XRD) analysis results for AC and Al-AC are displayed in Fig. 3(a). The characteristic peak of C and $CaCO_3$ appear at 2θ=26.64° and 29.42°, respectively. Compared with AC, eight characteristic peaks of Al_2O_3 were added to Al-AC at 2θ=

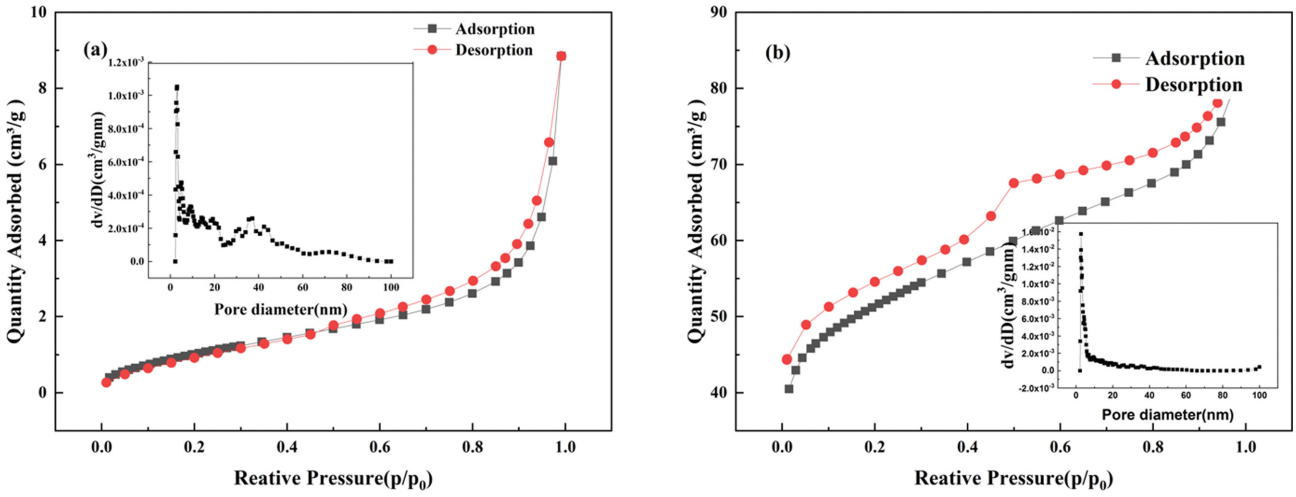

Fig. 2. N_2 adsorption/desorption analysis results for AC (a) and Al-AC (b).

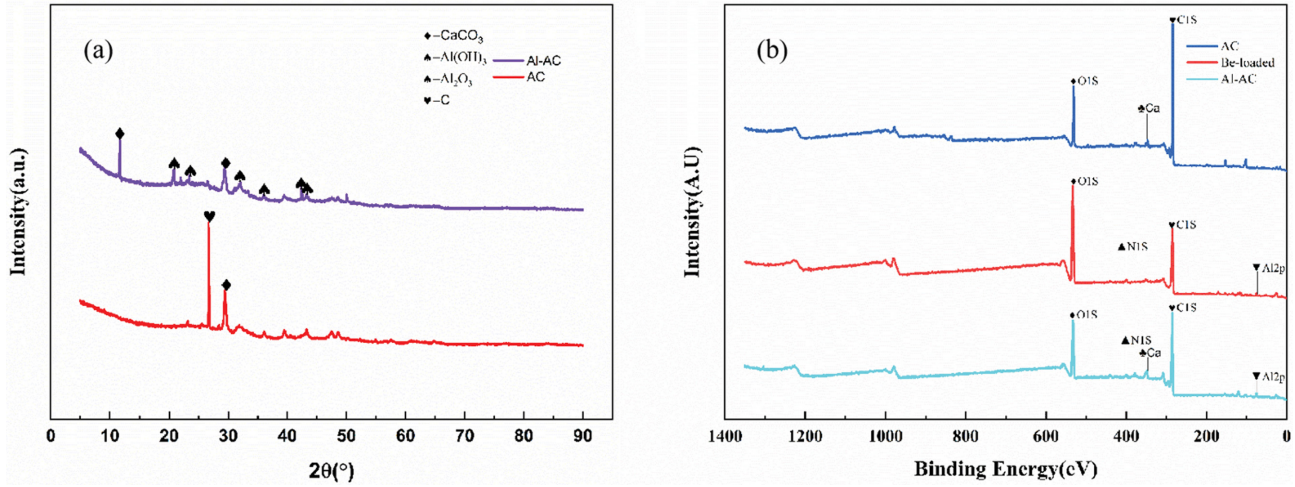

Fig. 3. XRD analysis of Al-AC and AC (a), XPS spectra of Al-AC before and after Be sorption (b).

Table 2. Proportion of elements before and after modification

Sample	Element	Weight (%)
AC	Al	0.66
	N	1.03
	C	86.10
	O	12.21
	Si	2.85
Al-AC	Al	5.28
	N	2.32
	C	62.13
	O	22.15
	Si	2.85

11.54°, 20.59°, 22.01°, 23.52°, 32.01°, 36.11°, 42.32°, and 43.25°, indicating that the modified carbon contains Al_2O_3 and $Al(OH)_3$. According to the preparation process of the Al-AC combined modified carbon, it was speculated that the following chemical reactions occurred during Al modification supported by AC: first, Al^{3+} and $Al(NO_3)_3$ were loaded on the AC. Second, Al_2O_3 and $Al(OH)_3$ were obtained by roasting at high temperatures [32].

1-4. XPS Analysis

XPS was used to investigate the mechanism of AC adsorption. Table 2 shows EDS analysis of AC and Al-AC. Fig. 3(b) shows the XPS analysis of AC and Al-AC. According to Fig. 3(b) and Table 2, the elemental composition of the Al-AC surface is 62.13% C, 5.28% Al, 22.15% O, 2.32% Si, and 2.85% N. Compared with AC, the proportion of Al and O elements increases, indicating that the surface of activated carbon is loaded with alumina, which is consistent with XRD results. The increased concentration of Al, N, and Ca atoms in Al-AC indicates that $Al(NO_3)_3$ successfully modified AC to analyze XPS peaked corresponding to O, Ca^{2+}, and Al^{3+} with high resolution. After adsorption, O increased significantly, indicating the precipitation mechanism [35]. Also, Ca^{2+} and Al^{3+} decreased indicated an ion-exchange mechanism. The binding energy of N was not reduced, indicating that Be did not react with the N groups or that Be insignificantly complexed with NH_3 and N [36].

2. Adsorption Studies

2-1. Surface Correspondence Analysis

The Design Expert 13.0.0 software (Stat-ease, Inc., Minneapolis, USA) was used to calculate the impact of each factor and its interaction. Eq. (1) shows that beryllium removal efficiency (Y) is a function of initial pH (X_1), Al^{3+} loading capacity (X_2), and adsorbent amount (X_3).

$$Y=-32.12889+25.86004*X_1+218.34624*X_2+13.37767*X_3 +8.68909*X_1*X_2+0.766738*X_1*X_3-14.47372*X_2*X_3 -2.01350*X_1^2-710.36489*X_2^2-2.60925*X_3^2 \quad (1)$$

F-value test was used to statistically judge the significance of each item in polynomial Formula (1), and variance analysis was conducted for the response surface quadratic model, as shown in Table 3. Table 3 shows that the F-value of this model is 93.64, the probability value is meager (<0.0001), and the determinant coefficient (R^2) value is 0.9917. The model interpretation shows that only 0.83% of the change response cannot be explained by the model, indicating that the fit is good enough [26].

Table 3 shows the significance, F-value and p-value of each coefficient. The more significant F-value is, the smaller p value is, and the more significant the corresponding coefficient is [37]. P-value less than 0.05 and 0.01 were statistically significant [38]. According to the established model (Formula 1), the interaction effects of initial pH (X_1), Al^{3+} loading capacity (X_2) and adsorbent dosage (X_3) and their response surfaces are shown in Fig. 1(a)-(c), respectively. Fig. 4 shows that the beryllium removal rate increases with the increase of pH and adsorbent dosage.

2-2. Effect of Al Ion Addition

The optimum adsorption conditions were selected by studying the adsorption effect of different ion additions on the modified AC. The additive amount of $Al(NO_3)_3$ is 5%, 10%, 15%, 20%, and 25% of the mass of AC, respectively. Fig. 5(a) shows that the effect was the best when the load metal content was 15%, whereas the adsorp-

Table 3. Analysis of variance (ANOVA) for the fitted quadratic polynomial model for optimization of Al-AC

Source	Sum of squares	Degree of freedom	Mean square	F value	p Value
Model	19,334.16	9	2,148.24	93.23	<0.0001
Initial pH (X_1)	10,582.02	1	10,582.02	459.22	<0.0001
Al^{3+} addition (X_2)	208.44	1	208.44	9.05	0.0197
Dosage (X_3)	63.55	1	63.55	2.76	0.1407
X_1X_2	63.93	1	63.93	2.77	0.1397
X_1X_3	74.18	1	74.18	3.22	0.1159
X_2X_3	31.05	1	31.05	1.37	0.2806
X_1^2	1,555.01	1	1,555.01	67.48	<0.0001
X_2^2	466.06	1	466.06	20.23	0.0028
X_3^2	108.15	1	108.15	4.69	0.0670
Residual	23.04	7	23.04		
Lack of fit	53.74	3	53.74	2,651.25	<0.0001
Pure error	0.0203	4	0.0203		
Cor total	0.0811	16			
R^2	0.9917				

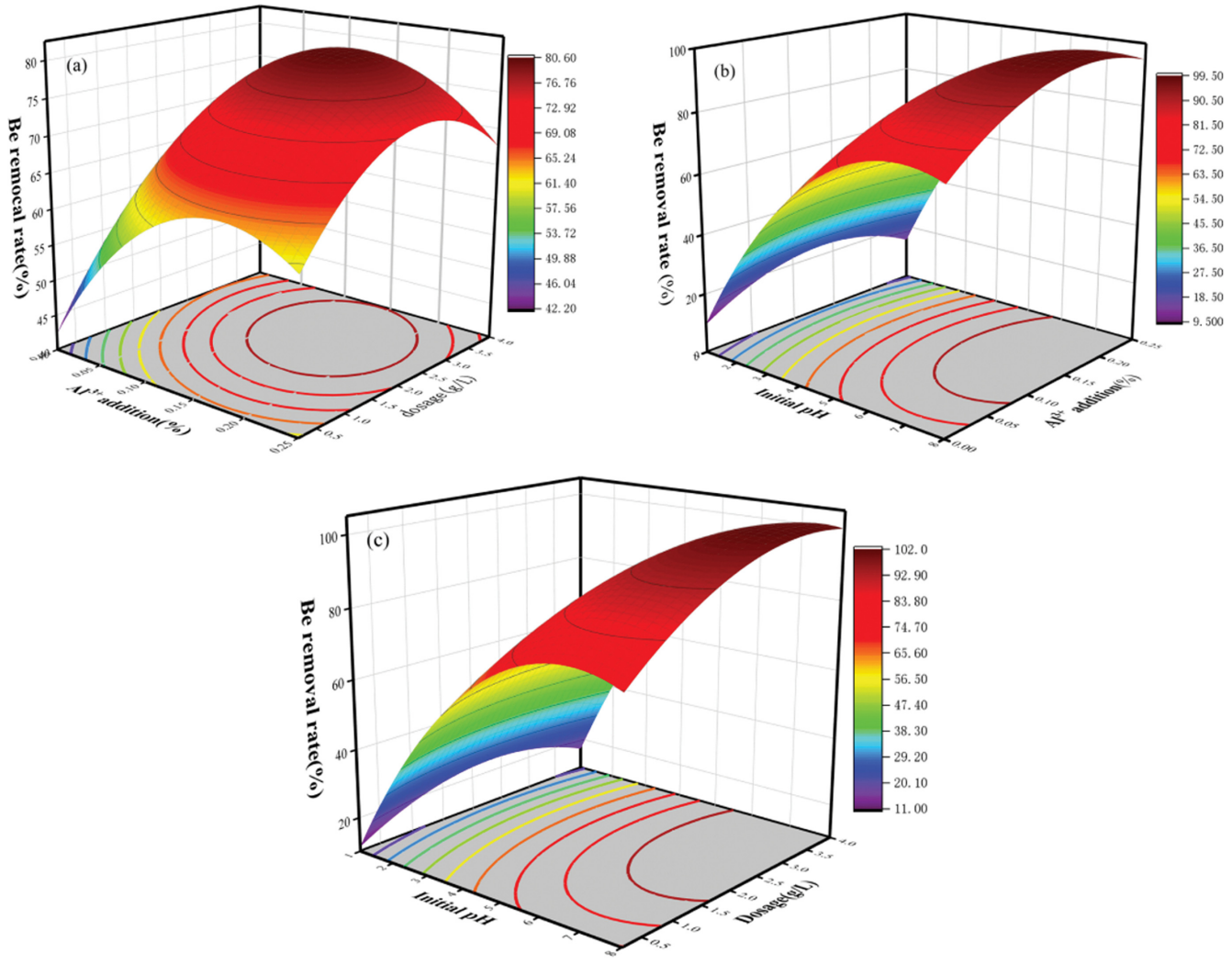

Fig. 4. Response surface graph for interactions between the factors.

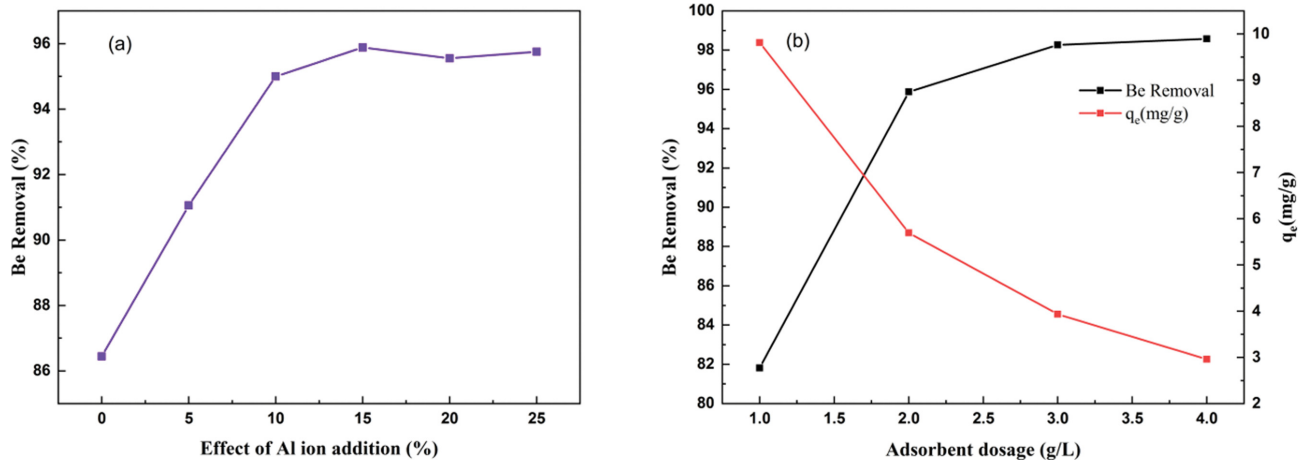

Fig. 5. Effect of Al Ion addition (a), effect of different amount of activated carbon on adsorption of Beryllium (b).

tion effect changed slightly when the load metal content reached 20% and 25%, indicating that the load metal content was saturated. When the loading amount was high, the adsorption capacity of the adsorbent changed insignificantly, indicating that the active site was occupied by loaded Al ions or intermediates, resulting in a slight change in the adsorption effect [39].

2-3. Effect of Biochar Dose on Adsorption

Under the condition of pH=6.0, the optimal amount of adsorbent was observed. A positive correlation exists between the amount of adsorbent and the adsorption effect (Fig. 5(b)). When the amount of adsorbent was 3 g/L, the removal rate exceeded 99%, the amount of adsorbent was negatively correlated with adsorption capacity and positively correlated with removal rate. Further increase in the adsorbent mass contributes slightly to the adsorption efficiency. The adsorption amount of Be was negatively related to the adsorption efficiency, which was due to the increase in the degree of unsaturation of the AC adsorption sites [36]. Therefore, the adsorbent dosage of 3 g/L was selected as optimum for further experiments.

2-4. Effect of Solution pH on Metal Adsorption

In the liquid phase, the pH is important for effective adsorbate-adsorbent interaction [28]. To explore the influence of different pH values on the adsorption performance, the effect of adsorbent on Be adsorption between pH=1.0-8.0 was analyzed under the conditions of an adsorbent dosage of 4-g/L, temperature of 25 °C, and initial Be concentration of 15 mg/L. The change in pH altered the physicochemical properties of the adsorbate and the physicochemical properties of the adsorbents. The $Be(OH)_2$ precipitation occurred when Be was between pH=6.5-10.0, which affected the removal rate of Be. The existing forms of its ions are shown in Table 4 [9]. Fig. 6(a) shows that Be began precipitating when the pH exceeded 6.0. When pH=1.0-6.0, the adsorption effect increased as the pH increased, and when the pH=6.0-8.0, the adsorption effect decreased as the pH increased and culminated at pH=6.0. The functional groups involved in the reaction may affect the adsorption efficiency The infrared spectral analysis showed that Al-AC had various functional groups, such as carboxyl, hydroxyl, and amine groups, most of which could produce a complex reaction with Be [36]. Under neutral and alkaline conditions, beryllium and carbonate ions will form $Be_2(OH)_2CO_3$ precipitation [40]. Additionally, at a low pH value, H^+ occupies the most active sites on the AC surface, resulting in electrical repulsion and reduced Be ion adsorption capacity [29].

To establish a reasonable adsorption mechanism, adsorption experiments were conducted, and the Zeta potential of Al-AC was measured at different pH values (Fig. 6(b)). The Zeta potential of Al-AC (Fig. 6(b)) indicates that there are many negative charges on the surface of the Al-AC particles within the pH range studied, and the surface charges increase as the pH increases. As the solution pH increases, the AC surface develops a negative charge due to the successive deprotonation of the positively charged groups on the surface [30], and the surface negative charge density increases. Thus, the electrostatic attraction is generated between the negative charge site of Al-AC and the Be compound. Due to electrostatic surface interaction, the adsorption of Be compounds on Al-AC increases as the solution pH increases.

2-5. Effect of Coexistent Metal Ions

Several metal cations exist in industrial wastewater, such as Al^{3+}, Fe^{2+}, Fe^{3+}, Cu^{2+}, Mn^{2+}, and Zn^{2+}. These metal ions may affect the adsorption effect. To explore the effect of metal cations on the adsorption capacity of Al-AC, the effects of different concentrations of metal ions (Fe^{2+}, Fe^{3+}, Cu^{2+}, Mn^{2+}, and Zn^{2+} concentrations of 10 to 40 mg/L) on the adsorption of Al-AC were investigated. Fig. 7 shows that the increase in Cu^{2+} concentration inhibits the adsorption effect of Al-AC. When the Cu^{2+} concentration was 40 mg/L, the adsorption of Be on AC decreased by 30%. The high concentration of Cu mainly exists in the form of ions and competes for the adsorption sites of Be^{2+} on the adsorbent [41]. Evidently, Fe^{2+}, Fe^{3+}, Mn^{2+}, and Zn^{2+} significantly affected the whole adsorption process, and the removal effect exceeded 99%. The addition of

Table 4. Equilibrium relationship between beryllium complexes

Number	Balance equation	Balance coefficient
1	$Be(OH)_2(s)+OH^-=HBeO^-+H_2O$	3.2×10^{-2}
2	$Be(OH)_2(s)+2OH^-=BeO_2^{2-}+2H_2O$	2.0×10^{-3}
3	$Be(OH)_2(s)+2H^+=Be^{2+}+2H_2O$	7.3×10^{6}

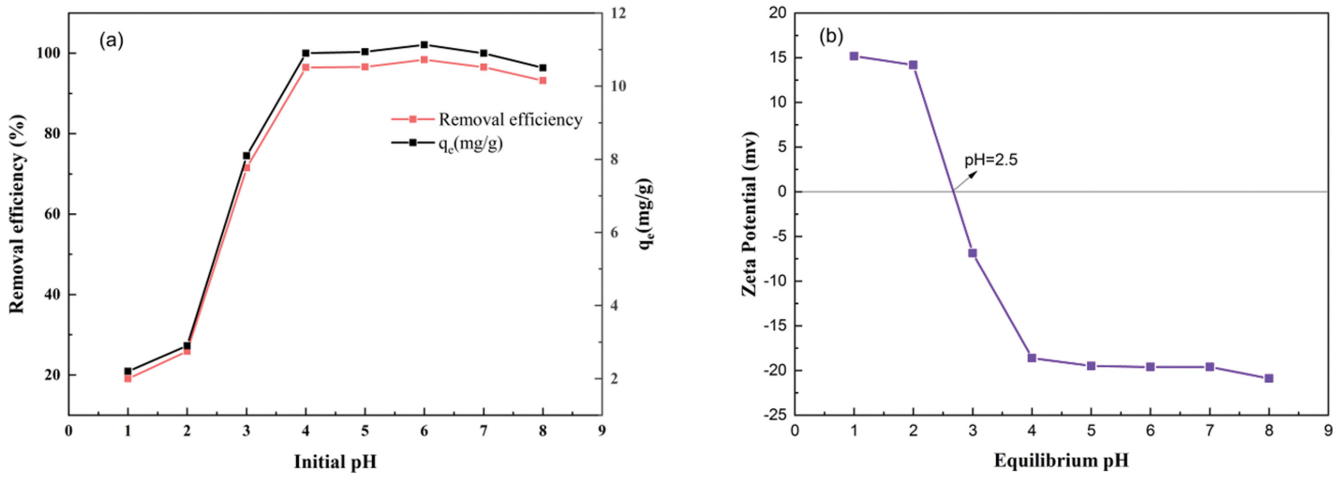

Fig. 6. Effect of different pH (a) and Zeta potentials (b) of the activated carbons.

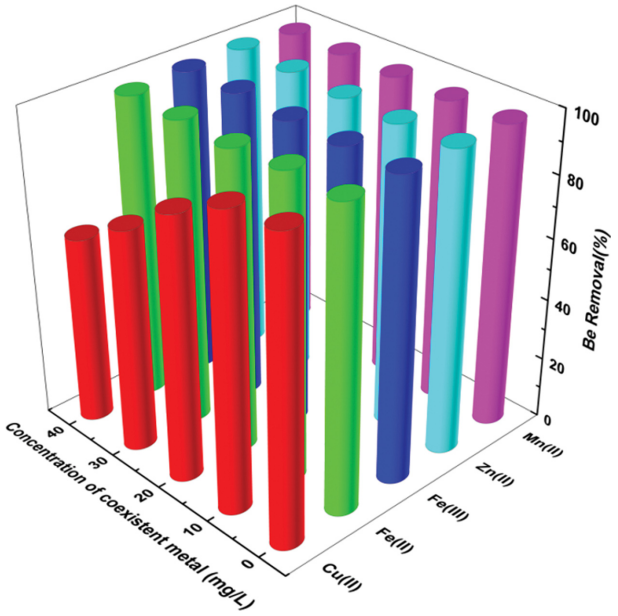

Fig. 7. Sorption of beryllium and coexistent metal ionsin binary metal systems.

Fe^{2+} and Fe^{3+} significantly improved the adsorption effect of Be because the $Fe(OH)_3$ colloid coprecipitated with Be at pH=6.0. The results agree with the results of Sun Fang [39].

Table 5. Kinetic models and adsorption isotherm models equations

Models	Equation	Reference
Pseudo-first-order model	$q_t = q_e(1-e^{-k_1 t})$	[34]
Pseudo-second-order model	$q_e = \frac{q_m k_L C_e}{1+k_L C_e}$	[42]
Intraparticle diffusion model	$q_t = k_s t^{1/2} + C$	[43]
Langmuir model	$q_e = \frac{q_m k_L C_e}{1+k_L C_e}$	[44]
Freundlich model	$q_e = k_F C_e^{1/n_F}$	[45]
Temkin model	$q_e = B\ln(a_t C_e)$	[46]

2-6. Adsorption Kinetics

Fig. 8 shows that the efficiency of Al-AC adsorption of Be(II) in the initial stage is very high, and the adsorption amount increases rapidly. Afterward, the adsorption rate decreased gradually and stabilized. In terms of the order of the rate constants, the kinetic analysis of the adsorption system is essential for understanding the adsorption kinetics [28]. At an initial pH=6.0, the kinetic data of the Be(II)/Al-AC system was analyzed.The equations are as follows Table 5.

The kinetic pseudo-first-order, pseudo-second-order, and intraparticle diffusion models were fitted to the experimental data, and

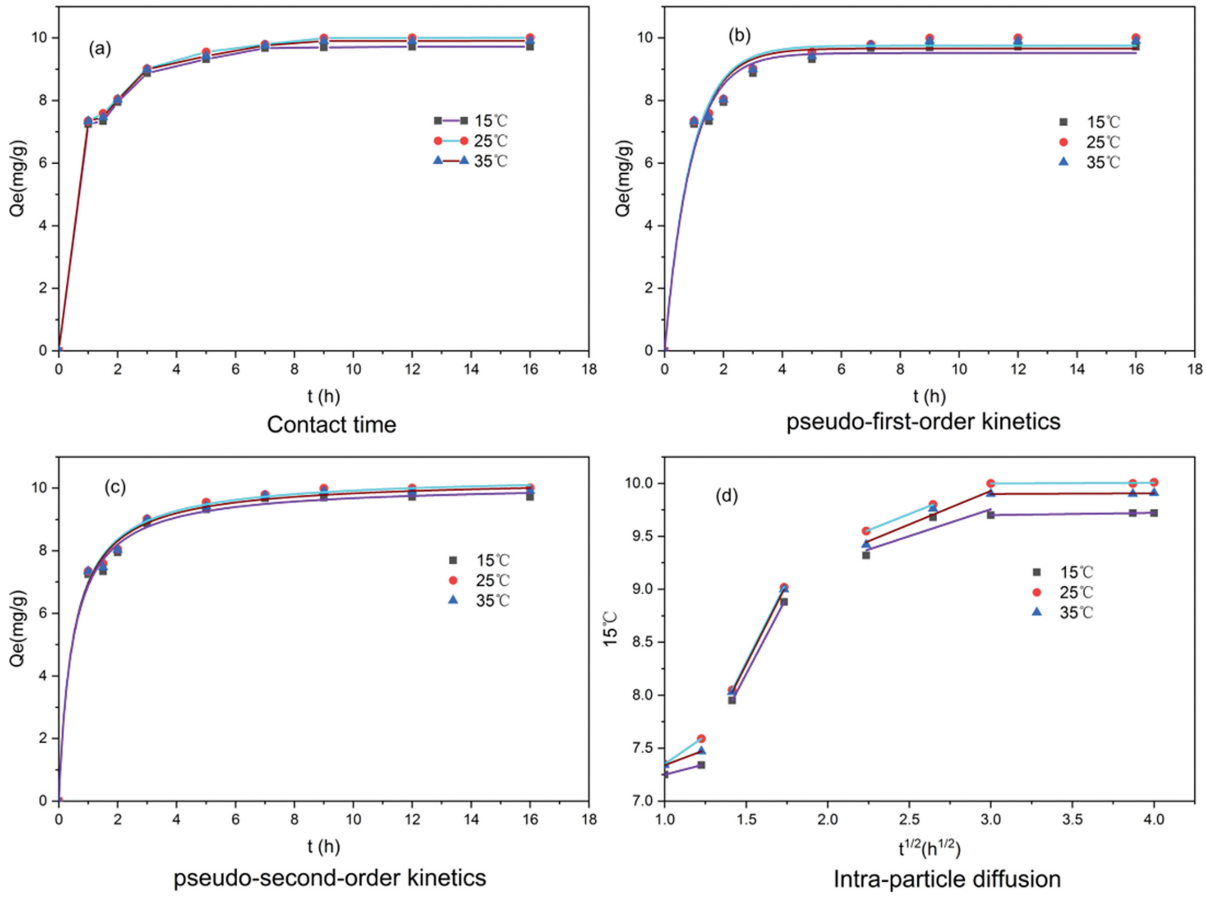

Fig. 8. Adsorption kinetics model fitting of Al-AC.

Table 6. Parameters of kinetic models for the adsorption of Be(II) onto Al-AC

T	Pseudo-first order				Pseudo-second order				Intra-particle diffusion model		
	q_e	k_1	R^2	RMSE	q_e	k_2	R^2	RMSE	k_s	C	R^2
15 °C	9.519	1.116	0.97876	0.19265	10.135	0.203	0.99423	0.04805	0.02108	6.85	0.9714
25 °C	9.753	1.128	0.97892	0.20889	10.556	0.197	0.99518	0.04773	0.00679	6.28	0.9982
35 °C	9.666	9.519	0.97876	0.19265	10.304	0.209	0.99470	0.05076	0.00637	6.76	0.9258

their nonlinear adjustments are shown in Fig. 8. The R^2 values (R_1^2=0.97892, R_2^2=0.99518, R_3^2=0.9982) and the residual root-mean squared error (RMSE) values listed in Table 6 show that the pseudo-second-order dynamics is more consistent at pH=6.0. Therefore, the adsorption of Be(II) on Al-AC is a combination of chemical and physical adsorption. The pseudo-second-order model indicates that the adsorption of Al-AC on Be(II) is mainly controlled by chemical adsorption, such as surface complexation and mineral coprecipitation [47]. The pseudo-second-order model showed a low desorption rate due to the effective interaction between the adsorbate and adsorbent [48]. The adsorption efficiency reached 95% at 2 h, indicating that there were many free adsorption sites in the early stage. Each adsorption condition had two linear stages. The first stage is associated with the transfer of Be(II) molecules from the liquid to the outer surface of Al-AC. The second stage is specified as the intra-particle diffusion model, where Be(II) molecules enter the porous structure of Al-AC [15]. AC and clay minerals are widely used to remove target pollutants in actual wastewater due to their moderate cost and strong adsorption capacity [49]. Evaluation of the adsorption performance of Al-AC in actual wastewater would be an important content of future work.

2-7. Adsorption Isotherm

Fig. 9 shows the effect of the initial concentration of Be(II) on the adsorption capacity of Al-AC. As the primary Be concentration increases, the adsorption amount of Be increases because the adsorption of Al-AC relates to the amount of Be. At a high Be concentration, the adsorption driving force of Al-AC increases; thus, the adsorption capacity increases [43].

The isotherm model can illustrate the adsorbate-adsorbent interaction [28]. The experimental equilibrium data of Be(II) adsorption at pH=6.0 were analyzed by the Langmuir, Freundlich, and Temkin models. The equations are as follows Table 5. Fig. 9 shows their nonlinear fittings, indicating the three kinds of adsorption isotherms of Al-AC. Table 7 shows the calculation parameters of the three isotherms. The Langmuir isotherm (R_2=0.989) was more consistent with the experimental data than the Freundlich (R_2=0.930) and Temkin (R_2=0.939) isotherms, indicating that the Langmuir isotherm better describes the adsorption behavior of Be by Al-AC.

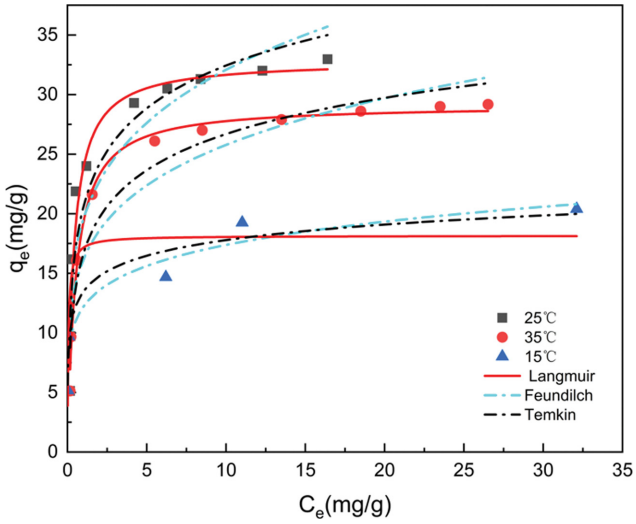

Fig. 9. Adsorption isotherms fitting of Al-AC.

The Langmuir equation applies to the homogeneous adsorption system, and the adsorption process is the monolayer adsorption, in which the adsorption of each adsorbent molecule had equal activated adsorption energy [53]. The Temkin model predicts that the heat of adsorption changes linearly, rather than logarithmically, as the adsorbent is covered [28]. Table 7 shows that the R^2 value of the Temkin model is 0.939, indicating that the model was relatively consistent with the experimental data. A Temkin constant (b_t) of <1.0 indicates that within the studied concentration range, the adsorption reaction of Al-AC on Be is endothermic [54], suggesting that mainly a chemical bond synthesis reaction occurred on the Al-AC surface. In the Freundlich model, the $1/n_F$ values at different temperatures were all <1.0, indicating that adsorption was feasible [55,56]. Overall, Al-AC showed a maximum monolayer adsorption capacity of 34 mg/g, which is excellent compared to several biological substrates and adsorbents used to adsorb Be(II) (Table 8).

2-8. Adsorption Thermodynamics

Adsorption thermodynamics is helpful to understand the ad-

Table 7. Parameters of isotherm models for the adsorption of Be(II) onto Al-AC

T	Langmuir			Freundlich			Temkin		
	K_L	Q_m	R^2	K_F	$1/n_F$	R^2	a_t	b_t	R^2
15 °C	17.0091	18.152	0.83964	18.152	0.15404	0.93085	1,262.28	0.000786	0.93617
25 °C	2.6247	32.860	0.98915	16.116	0.21596	0.81609	53.0908	0.00213	0.8806
35 °C	1.89988	29.226	0.92932	19.514	0.20387	0.8642	44.5376	0.00174	0.93934

Table 8. Comparison of maximum monolayer adsorption and removal rate of Be(II) on various biomass-derived activated carbons

Precursor	pH	q_m (mg g^{-1})	Removal rate%	Reference
Chlorella vulgaris Immobilized	6.5	--	80	[7]
Bacterial cells	6.0	--	80	[8]
Chitosan modified zeolite	7-9	0.252	90.1	[50]
Metal oxide nanoparticles	1.0	--	80	[25]
Modified chitosan resin	1.0	44.96	--	[51]
Polystyrene-based chelating	8.0	22.5	98	[52]
Kaolinite powder	6.0	0.2461	92.36	[12]
Aerobic granule	7.5-8	14	82	[39]
Activated sludge	5.0	0.6849	99	[6]
Al-AC	6.0	32.86	99	This study

sorption mechanism. Eq. (2) can be used to calculate the distribution coefficient K_d of Be on Al-AC.

$$K_d = \frac{q_e}{C_e} \quad (2)$$

In Eq. (2), the units of C_e and q_e are mg/L and mg/g, respectively. Since the unit of K_d is L/g, it cannot be directly used to calculate ΔG^0, ΔH^0, and ΔS^0. K_c is obtained by multiplying K_d by 1,000 [57,58]. The relevant equation is as follows:

$$K_c = 1{,}000 K_d \quad (3)$$

$$\Delta G^0 = -RT\ln K_C \quad (4)$$

$$\ln(K_C) = -\frac{\Delta H^0}{RT} + \frac{\Delta S^0}{R} \quad (5)$$

Thermodynamic parameters, such as ΔG^0, ΔH^0, and ΔS^0, could provide the theoretical basis for evaluating the change in adsorption heat [23]. The thermodynamic adsorption parameters of Al-AC are calculated in Table 8. ΔG^0 indicates the spontaneity of the adsorption process and the reactions involved. ΔG^0 of Al-AC adsorption of Be was <zero, indicating that the adsorption of Be by Al-AC was mainly chemical, and the experimental process was spontaneous [52]. ΔS^0 measures the amount of entropy between atoms. ΔS^0 of the Al-AC-adsorbed Be exceeded zero, indicating that the disorder degree of the solid-liquid interface increased after Al-AC adsorbed Be [59]. ΔH^0 determines whether the reaction absorbs or releases energy [33]. ΔH^0 of the Al-AC adsorption of Be exceeded zero, indicating an endothermic reaction, consistent with the adsorption isotherm model. This result further verifies the experimental results that the adsorption capacity of Al-AC increases as temperature increases.

2-9. Desorption of Be Metal Ion from Al-AC

Different molar concentrations of nitric, sulfuric, hydrochloric acids, and sodium hydroxide were employed for desorption [50] and the equations were shown in Table 9. After adsorption, 0.1-g Al-AC was placed in 25 mL eluent and stirred for 2 h. The elution efficiency was improved by using 3 M hydrochloric acid and sodium hydroxide. The experimental results show that Be ions' effective desorption rate in 3 M hydrochloric acid solution was ~84% within 2 h. The desorption efficiency is 87.5% in 10% NaOH solution. As Al-AC is an alkaline adsorbent, 3 M hydrochloric acid will destroy its structure in the cycle experiment, resulting in a secondary adsorption efficiency of only 2%, while 10% sodium hydroxide can desorb beryllium well and enrich it on the premise of protecting the Al-AC structure. As shown in Fig. 10, the desorption efficiency increases with the number of cycles, and the removal rate was above 80% in six cycles, proving that the Al-AC has excellent cycling performance.

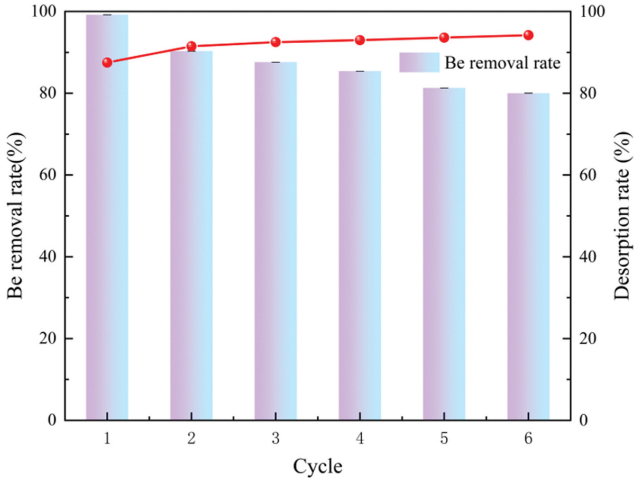

Fig. 10. Be removal rate and desorption rate of Al-AC.

Table 9. Desorption equations

	Equation	Reference
Desorption	$q_e de = \frac{(C_e de)V}{W}$	[60]
	$DE(\%) = \frac{(q_e de)100}{q_e ad}$	[50]

3. Analysis of Al-AC Adsorption Mechanism

3-1. SEM Analysis of Samples Before and After Adsorption

Fig. 11 shows the surface changes after the activation process in AC and Al-AC SEM images. Fig. 11(d) shows apparent differences in Al-AC surface topography, and the content of Al in Al-AC increased obviously, indicating that Al was loaded on the AC surface. Fig. 11(e) shows that many substances accumulate on the AC surface and in the pores after adsorption [17]. Besides, the surface of

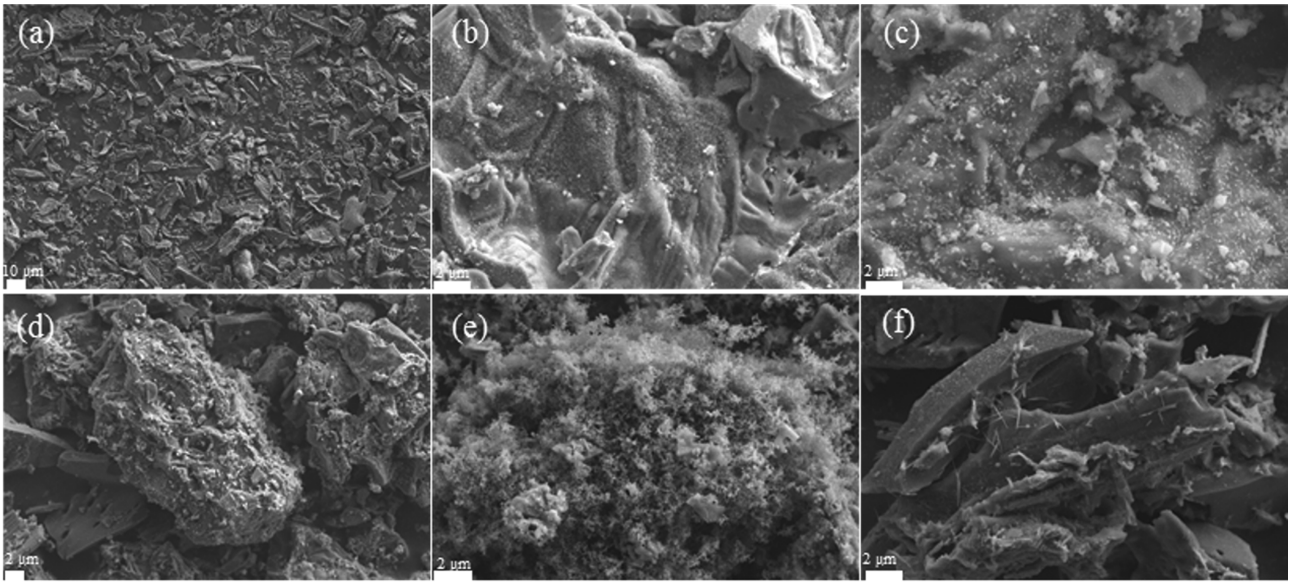

Fig. 11. SEM analysis of (a) (b) before adsorption and adsorption (c) of AC, (d) before adsorption and adsorption (e) of (15% Al-AC) and (f) before adsorption (25% Al-AC).

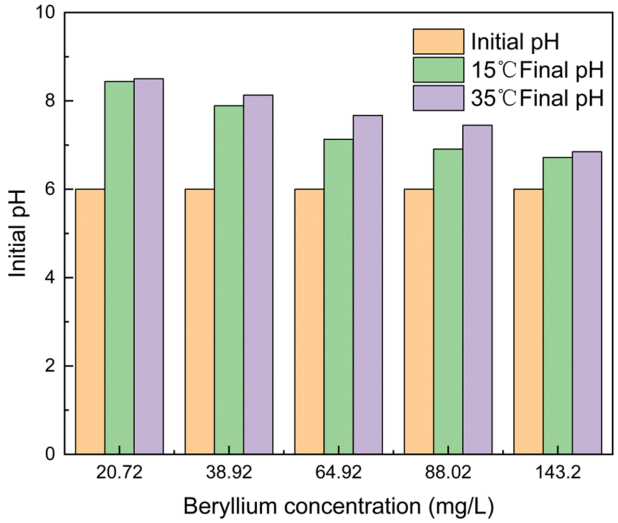

Fig. 12. The change of pH before and after carbon adsorption.

the adsorbent appears irregular and porous. Thus, it could be concluded that the adsorbent had sufficient morphology for adsorbing Be^{2+}.

Additionally, Al-AC had a rough surface and cavities of different sizes, indicating that the porous structure was well developed due to the nitric acid activation and high-temperature roasting. The surface pores of Al-AC provided appropriate channels for Be molecules to enter the carbon structure, mesopores, and micropores and combine with surface functional groups.

3-2. Mechanism

The kinetic and thermodynamic analysis of Al-AC indicated that the adsorption of Be by Al-AC is complex. The comprehensive adsorption mechanism is shown in Fig. 13, and the adsorption of Be on the modified carbon is both mainly physical and chemical, which manifests in the liquid film diffusion, micropore diffusion, electrostatic attraction, and ion exchange of Be^{2+} on the Al-AC surface.

The ionic states of the active functional groups of the adsorbents and Be depend mainly on the aqueous solution pH. Therefore, the solution pH determined the primary mechanism of Be adsorption on the Al-AC surface. Electrostatic attraction significantly affected the adsorption of Be(II) cations on the negatively charged surface of the adsorbent under neutral conditions. Fig. 12 shows that the solution pH increases before and after adsorption, and the pH change decreases as the concentration increases, indicating an alkaline adsorbent and the release of OH^- to coprecipitate with Be. The influence of ionic strength on the adsorption system shows that Be ions mainly form covalent bonds with the adsorbent surface under a neutral condition. The effect of the solution pH also confirmed the ion exchange of Be on Al-AC. The XRD and XPS analyses, adsorption isotherm model, and desorption test showed that the adsorption of Be(II) on Al-AC occurs mainly through ion exchange, electrostatic interaction, and precipitation reaction. Additionally, the intraparticle diffusion indicated that the adsorption of Be(II) on the surface of Al-AC was controlled by membrane diffusion, which confirmed the chemisorption of Be(II) on the Al-AC surface.

CONCLUSIONS

The lotus-leaf-derived carbon modified with $Al(NO_3)_3$ had a higher specific surface area, and the adsorption effect of Be was significantly enhanced. According to the characterization, the specific surface area increased from 4.3573 to 155.87 m^2/g. The adsorption kinetics and isotherms showed that the pseudo-second-order kinetics and Langmuir model could better fit the adsorption process of Be by Al-AC in Be(II)/Al-AC AC systems. The optimal adsorption conditions of Al-AC were as follows: pH=6.0, tempera-

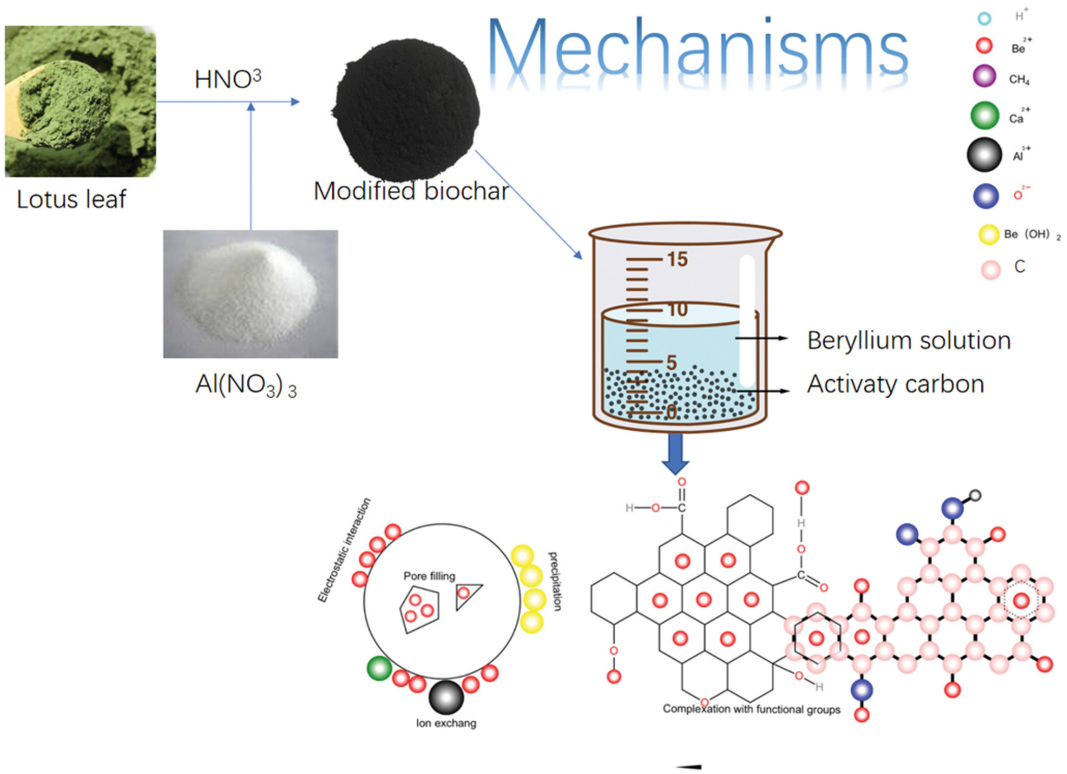

Fig. 13. Al-AC adsorption mechanism diagram.

ture of 25 °C, 3-g/L adsorbent, and 5-h equilibrium adsorption time. The maximum adsorption capacity of Al-AC was 32.86 mg/g, and the maximum adsorption rate was 99%. The adsorption process of Al-AC was mainly based on chemical adsorption. In addition to The influence of Cu^{2+} on the adsorption process of beryllium, all kinds of coexisting ions promote the effect of adsorption. Additionally, the industrial wastewater treatment pH is neutral, which is very consistent with the treatment range of Al-AC. Therefore, Al-AC AC can be considered a potential precursor for producing AC, with great potential for adsorbing Be from aqueous solutions.

ACKNOWLEDGEMENTS

We thank the following funding agencies for supporting this work: Foundation of State Key Laboratory of Nuclear Resources and Environment (2020NRE02). Research on characteristic properties of typical radioactive solid waste and radiation protection regulation technology and operation management mechanism (2019YFC1907701).

REFERENCES

1. T. Xiangyuan, X. Lei, W. Rucheng, Z. Rongqing, H. Huan and L. Chen, *J. Nanjing University (Natural Science)*, **56**, 815 (2020).
2. L. Chengxing, *Engineering study on biological treatment of beryllium-containing wastewater*, Master dissertation, Central South University (2010).
3. M. Tanveer and L. Wang, *Plant Physiol. Bioch.*, **139**, 691 (2019).
4. M. L. Chiarappa-Zucca, R. C. Finkel, R. E. Martinelli, J. E. McAninch, D. O. Nelson and K. W. Turteltaub, *Chem. Res. Toxicol.*, **17**, 1614 (2004).
5. B. Vladimír, V. Elena and V. Symon Karel, *Environ. Res.*, **22**, 439 (1980).
6. Z. Minglong, C. Liyuan, M. Xiaobo, L. Qingzhu and W. Shunwen, *Technol. Water Treat.*, **32**, 45 (2006).
7. L. Phillip, *J. Environ, Sci. Heal A.*, **25**, 21 (2008).
8. L. C. Robles and A. J. Aller, *Quim. Anal.*, **15**, 21 (1995).
9. J. Ke, Z. Kanggen and Y. Youcai, *Nonferrous Metal (Smelting Section)*, **06**, 83 (2018).
10. X. Xuejun and L. Yanhui, *Chinese J. Rare Metals.*, **S1**, 59 (2007).
11. C. Hewen, Z. Xiaojia, X. Haiying and Y. Xiaorong, *Water Technol.*, **06**, 16 (2011).
12. W. Minzhan, Z. Zhengke, C. Sili, C. Sha, G. Qingwei and W. Jinsong, *Technol. Water Treat.*, **47**, 78 (2021).
13. K. Ersin, B. Sezgin and Y. Mehmet, *Food Addit Contam Part A Chem. Anal. Control Expo. Risk Assess.*, **28**, 455 (2011).
14. D. Yongbo, X. Lei, Q. Zhimin and S. Honglan, *Chemosphere*, **262**, 127940 (2021).
15. L. Xianchun, W. Huanran and S. Gege, *Int. J. Hydrogen Energ.*, **144**, 25265 (2019).
16. S. Norouzi, M. Heidari, V. Alipour and K. Dindarloo, *Bioresour. Technol.*, **258**, 48 (2018).
17. F. Sabrina. Lütke, V. Andrei. Igansi, L. Pegoraro and R. s. Tito, *J. Environ. Chem. Eng.*, **17**, 103396 (2019).
18. L. Lin, L. Suqin and L. Junxin, *J. Hazard. Mater.*, **192**, 683 (2011).
19. Y. Kuang, Z. Xiaoping and Z. Shaoqi, *Water*, **12**, 587 (2020).
20. A. S. Zulaicha, *J. Phys. Conf. Ser.*, **1**, 1751 (2021).
21. L. Youji, L. Jing, M. Mingyuan and Y. Wenbin, *Sci. China Ser. B.*,

52, 1113 (2009).
22. P. Karthikeyan and S. Meenakshi, *J. Mol. Liq., C*, **296**, 111766 (2019).
23. R. Zhijun, J. Biao, Z. Guangming and L. Longyi, *Chemosphere*, **262**, 127895 (2021).
24. K. A. Al-Saad, M. A. Amr, D. T. Hadi, R. S. Arar, M. M. AL-Sulaiti, T. A. Abdulmalik, N. M. Alsahamary and J. C. Kwak, *Arab. J. Nucl. Sci. Appl.*, **45**, 335 (2012).
25. B. Kotaro, K. Naoki, S. Saki and M. Hideaki, *Anal. Sci.*, **11**, 1067 (2014).
26. Y. Yücel and S. Göycıncık, *Waste Biomass Valori*, **6**, 1077 (2015).
27. E. Maria Iannicelli-zubiani, P. Gallo Stampino, C. Cristiani and G. Dotelli, *Chem. Eng. J.*, **341**, 75 (2018).
28. O. Pezoti, A. L. Cazetta, K. C. Bedin, L. S. Souza, A. C. Martins, T. L. Silva and V. C. Almeida, *Chem. Eng. J.*, **288**, 778 (2016).
29. A. C. Martins, O. Pezoti, A. L. Cazetta and V. C. Almeida, *Chem. Eng. J.*, **288**, 291 (2015).
30. P. Senthil Kumar, S. Ramalingam, S. D. Kirupha and S. Sivanesan, *Chem. Eng. J.*, **167**, 122 (2010).
31. A. Oberlintner, V. Shvalya, A. Vasudevan, D. Vengust, B. Likozar, U. Cvelbar and U. Novak, *Appl. Surf. Sci.*, **581**, 152276 (2022).
32. M. Thommes, *Pure Appl. Chem.*, **87**, 1051 (2016).
33. L. Weifeng, Z. Jian, Z. Chenglu and L. Ye, *Chem. Eng. J.*, **162**, 677 (2010).
34. Z. Heshan, G. Wanqian, L. Shuo and C. Jo-shu, *Bioresour. Technol.*, **244**, 1456 (2017).
35. T. Watanabe, Y. Miki, T. Masuda, H. Kanai, S. Hosokawa, K. Wada and M. Inoue, *Appl. Catal. A-gen.*, **396**, 140 (2011).
36. T. Depci, *Chem. Eng. J.*, **181**, 467 (2012).
37. I. Abdulkadir, B. S. Mohammed, M. S. Liew and M. M. A. Wahab, *Case Stud. Constr. Mat.*, **14**, E00525 (2021).
38. S. Çam Kaynar and Ü. H. Kaynar, *Nucl. Sci. Tech.*, **30**, 75 (2019).
39. S. Fang, S. Wei-ling, S. Hai-mei and N. Jin-ren, *Chem. Eng. J.*, **172**, 783 (2011).
40. V. S. Savenko, *Russ. J. Inorg. Chem.*, **52**, 465 (1965).
41. Y. Chenhui, Z. Yongqing, D. Meimei, D. Xiaodong and H. Shaobin, *Chem. Eng. J.*, **362**, 262 (2019).
42. Z. Peizhen, Z. Xiaoxiao, Y. Xiangru, X. Ruyue and H. Lujia, *Bioresour. Technol.*, **331**, 125013 (2021).
43. C. Yaoning, L. Meiling, L. Yuanping, L. Yihuan, C. Yanrong, L. Hui and L. Chen, *Bioresour. Technol.*, **321**, 12443 (2021).
44. H. Karaca, E. Altıntığ, D. Türker and M. Teker, *J. Disper. Sci. Technol.*, **39**, 1800 (2018).
45. F. Mashkoor, A. Nasar, I. Abdullah and M. Asiri, *Sci. Rep-uk.*, **8**, 8314 (2018).
46. M. Shaban, M. R. Abukhadra, M. G. Shahien and A. A. P. Khan, *Environ. Sci. Pollut. R.*, **24**, 18135 (2017).
47. C. Huayi, L. Wenyan, W. Jinjin and Z. Yulong, *Bioresour. Technol.*, **292**, 12198 (2019).
48. Z. Xin, L. Yaru, W. Mengru, P. Yao, H. Zhenbing, H. Mian and C. Zhihua, *Bioresour. Technol.*, **320**, 124264 (2021).
49. Z. Xiaogang, H. Xinyue, P. Hao, W. Jing and L. Sihao, *Bioresour. Technol.*, **334**, 125238 (2021).
50. R. Gang, Y. Yan, Y. Zhixin, D. Yaomin and L. Xiaoyi, *J. Saf. Environ.*, **16**, 208 (2016).
51. M. O. Abd El-magied, A. Mansour, F. A. Al Ghani Alsayed and S. Abd Eldayem, *J. Disper. Sci. Technol.*, **39**, 1597 (2018).
52. N. N. Basargin and O. V. Miroshnichenko, *Russ. J. Inorg. Chem.*, **57**, 758 (2012).
53. A. B. Petriciolet, D. I. M. Castillo and H. E. R. Ávila, *Adsorption processes for water treatment and purification*, Springer, Publications, Berlin (2017).
54. M. Hadi, M. R. Samarghandi and G. Mckay, *Chem. Eng. J.*, **160**, 408 (2010).
55. A. S. Singha and A. Guleria, *J. Environ. Chem. Eng.*, **2**, 1456 (2014).
56. S. Srivastava, S. B. Agrawal and M. K. Mondal, *Korean. J. Chem. Eng.*, **33**, 567 (2016).
57. S. Mirzaeei, F. H. Pirhayati, G. Mohammadi, E. Rahimpour, F. Martinez and A. Jouyban, *Phys. Chem. Liq.*, **57**, 788 (2019).
58. L. Jiayang, H. Changwei and H. Qingguo, *Bioresour. Technol.*, **271**, 487 (2018).
59. L. Yu and L. Ya-juan, *Sep. Purif. Technol.*, **61**, 229 (2007).
60. M. Barkat, D. Nibou, S. Chegrouche and A. Mellah, *Chem. Eng. Process.*, **48**, 38 (2007).